Characterization of the Tryptophan Fluorescence from Sarcoplasmic Reticulum Adenosinetriphosphatase by Frequency-Domain Fluorescence Spectroscopy†

Ignacy Gryczynski, Wieslaw Wiczk, Giuseppe Inesi, Thomas Squier, and Joseph R. Lakowicz*

Department of Biological Chemistry, School of Medicine, University of Maryland, 660 W. Redwood Street, Baltimore, Maryland 21201

Received July 28, 1988; Revised Manuscript Received December 14, 1988

ABSTRACT: We examined the tryptophan decay kinetics of sarcoplasmic reticulum Ca^{2+}-ATPase using frequency-domain fluorescence. Consistent with earlier reports on steady-state fluorescence intensity, our intensity decays reveal a reproducible and statistically significant 2% increase in the mean decay time due to calcium binding to specific sites involved in enzyme activation. This Ca^{2+} effect could not be eliminated with acrylamide quenching, which suggests a global effect of calcium on the Ca^{2+}-ATPase, as opposed to a specific effect on a single water-accessible tryptophan residue. The tryptophan anisotropy decays indicate substantial rapid loss of anisotropy, which can be the result of either intramolecular energy transfer or a change in segmental flexibility of the ATPase protein. Energy transfer from tryptophan to TNP-ATP in the nucleotide binding domain, or to IEADANS on Cys-670 and -674, indicates that most tryptophan residues are 30 Å or further away from these sites and that this distance is not decreased by Ca^{2+}. In light of known structural features of the Ca^{2+}-ATPase, the tryptophan fluorescence changes are attributed to stabilization of clustered transmembrane helices resulting from calcium binding.

High-affinity calcium binding to the sarcoplasmic reticulum ATPase is a specific requirement for activation of this enzyme, whereby ATP is utilized by formation of a phosphorylated enzyme intermediate, followed by translocation of the bound calcium and hydrolytic cleavage of P_i[1] [for review, see Inesi (1985)]. In parallel with functional activation, a structural effect of calcium is suggested by a small (3–4%) increase in the intrinsic tryptophan fluorescence of the ATPase protein (Dupont, 1976). The fluorescence effect is of interest since its Ca^{2+} concentration dependence and kinetic profile are consistent with those of enzyme activity (Guillain et al., 1982; Fernandez-Belda et al., 1984). However, the nature of the structural change (if any) revealed by the fluorescence rise remains to be determined. Its interpretation is rendered more complex by the number (13) of tryptophan residues present in each ATPase molecule (MacLennan, 1985). We are here reporting the results of further characterization of the Ca^{2+} effect on the fluorescence, obtained by analysis of frequency-domain fluorescence data. We also report measurements of tryptophan fluorescence anisotropy decays, quenching with acrylamide, and energy transfer between tryptophan residues and the fluorescent nucleotide analogue TNP-AMP or an IEADANS label placed on cysteine residues 670 and 674 of the ATPase protein.

Theory

Decays of Fluorescence Intensity. The frequency-domain data were analyzed by the method of nonlinear least squares (Gratton et al., 1984; Lakowicz et al., 1984). The measured data are compared with values predicted from a model, and the parameters of the model are varied to yield the minimum deviations from the data. For the case of a multiexponential decay, the impulse response $I(t)$ is given by

$$I(t) = \sum_i \alpha_i e^{-t/\tau_i} \tag{1}$$

where α_i is the preexponential factor and τ_i is the decay time. The fractional intensity of each component in the decay is given by

$$f_i = \frac{\alpha_i \tau_i}{\sum_j \alpha_j \tau_j} \tag{2}$$

Alternatively, the intensity decays can be modeled with a distribution of decay times (Alcala et al., 1987; James et al., 1987; Lakowicz et al., 1987b). We assumed that the individual components were distributed as a Lorentzian:

$$\alpha_i^\circ(\tau) = \frac{1}{\pi} \frac{\Gamma/2}{(\tau - \bar{\tau})^2 + (\Gamma/2)^2} \tag{3}$$

where Γ is the full width at half-maximum, $\bar{\tau}$ is the central value of the distribution, and $\int \alpha_i^\circ(\tau) = 1$. Hence, $\alpha_i^\circ(\tau)$ is a shape factor for the ith component in the distribution. In the case of two or more components, the distribution is given by

$$\alpha(\tau) = \sum_i g_i \alpha_i^\circ(\tau) = \sum_i \alpha_i(\tau) \tag{4}$$

where g_i represents the amplitude of the ith component (Lakowicz et al., 1987a,b). The intensity decay is then given by

$$I(t) = \int_{\tau=0}^{\infty} \alpha(\tau) e^{-t/\tau}\, d\tau \tag{5}$$

We also used energy transfer to determine the distribution of distances from tryptophan residues to specific sites on the ATPase. In this case the intensity decay is given by

† Supported by Grants HL-27867 (G.I.) and GM-35154 (J.R.L.) from the National Institutes of Health and Grants DMB-8502835 and DMB-8511065 (J.R.L.) from the National Science Foundation. This work was performed with the facilities at the Center for Fluorescence Spectroscopy (NSF DIR-8710401). J.R.L. acknowledges the support of the Medical Biotechnology Center, University of Maryland.

[1] Abbreviations: NATA, *N*-acetyl-L-tryptophanamide; Trp, tryptophan; ATPase, sarcoplasmic reticulum ATPase; TNP-ATP, 2′,3′-*O*-(2,4,6-trinitrocyclohexadienylidene)adenosine 5′-triphosphate; IEADANS, 5-[[[(iodoacetyl)amino]ethyl]amino]naphthalene-1-sulfonic acid; P_i, phosphate.

0006-2960/89/0428-3490$01.50/0

$$I_{DA}(t) = \int_{r=0}^{\infty} P(r) \sum_i \alpha_{Di} \exp\left[-\frac{t}{\tau_{Di}} - \frac{t}{\tau_{Di}} \left(\frac{R_0}{r} \right)^6 \right] \quad (6)$$

where α_{Di} and τ_{Di} are the intensity decay parameters found in the absence of energy transfer. These parameters are recovered from the multiexponential model (eq 1) in the absence of an acceptor and are held constant during the distance distribution analysis. The distance distribution was modeled as a Gaussian:

$$P(r) = \frac{1}{\sigma\sqrt{2\pi}} \exp\left[-\frac{1}{2} \left(\frac{r - \bar{r}}{\sigma} \right)^2 \right] \quad (7)$$

where $\bar{r}$ is the average and σ is the standard deviation of the distribution. The widths of the distribution are reported as the full width at half-maximum, which is given by $hw = 2.354\sigma$. Additional details are available elsewhere (Lakowicz et al., 1987a,b, 1988a).

Irrespective of the model assumed for the intensity decay, the frequency-domain data can be calculated from the sine and cosine transforms of $I(t)$:

$$N_\omega = \frac{\int_0^\infty I(t) \sin \omega t \, dt}{\int_0^\infty I(t) \, dt} \quad (8)$$

$$D_\omega = \frac{\int_0^\infty I(t) \cos \omega t \, dt}{\int_0^\infty I(t) \, dt} \quad (9)$$

where ω is the circular modulation frequency ($2\pi \times$ frequency in hertz). The calculated (c) values of the phase angle ($\phi_{c\omega}$) and the demodulation ($m_{c\omega}$) are given by

$$\tan \phi_{c\omega} = N_\omega / D_\omega \quad (10)$$

$$m_{c\omega} = (N_\omega^2 + D_\omega^2)^{1/2} \quad (11)$$

The parameters (α_i and τ_i; g_i, $\bar{\tau}_i$, and Γ_i; or $\bar{r}$ and hw) are varied to yield the best fit between the data and the calculated values, as indicated by a minimum value for the goodness-of-fit parameter χ_R^2:

$$\chi_R^2 = \frac{1}{\nu} \sum_\omega \left(\frac{\phi_\omega - \phi_{c\omega}}{\delta\phi} \right)^2 + \frac{1}{\nu} \sum_\omega \left(\frac{m_\omega - m_{c\omega}}{\delta m} \right)^2 \quad (12)$$

where ν is the number of degrees of freedom and $\delta\phi$ and δm are the uncertainties in the phase and modulation values, respectively.

Decays of Fluorescence Anisotropy. Suppose the sample is excited with a δ-function pulse of vertically polarized light. The decays of the parallel and perpendicular components of the emission are given by

$$I_\parallel(t) = \frac{1}{3} I(t)[1 + 2r(t)] \quad (13)$$

$$I_\perp(t) = \frac{1}{3} I(t)[1 - r(t)] \quad (14)$$

where $r(t)$ is the time-resolved anisotropy. Generally, $r(t)$ can be described as a multiexponential decay:

$$r(t) = r_0 \sum_i g_i e^{-t/\theta_i} \quad (15)$$

where r_0 is the limiting anisotropy in the absence of rotational diffusion, θ_i is the individual correlation time, and g_i is the associated amplitude. In the frequency domain the measured quantities are the phase angle difference Δ_ω between the perpendicular ($\phi_\perp$) and parallel ($\phi_\parallel$) components of the modulated emission ($\Delta_\omega = \phi_\perp - \phi_\parallel$) and the amplitude ratio Λ_ω of the parallel ($m_\parallel$) and perpendicular ($m_\perp$) components of the modulated emission ($\Lambda_\omega = m_\parallel / m_\perp$). These values are compared with those expected for an assumed anisotropy decay law.

The expected values of Δ_ω ($\Delta_{c\omega}$) and Λ_ω ($\Lambda_{c\omega}$) can be calculated from the sine and cosine transforms of the individual polarized decays (eq 13 and 14). The frequency-dependent values of $\Delta_{c\omega}$ and $\Lambda_{c\omega}$ are given by

$$\Delta_{c\omega} = \arctan \frac{D_\parallel N_\perp - N_\parallel D_\perp}{N_\parallel N_\perp + D_\parallel D_\perp} \quad (16)$$

$$\Lambda_{c\omega} = \left(\frac{N_\parallel^2 + D_\parallel^2}{N_\perp^2 + D_\perp^2} \right)^{1/2} \quad (17)$$

where N and D are calculated at each frequency. The parameters describing the anisotropy decay are obtained by minimizing the squared deviations between measured and calculated values, with an expression analogous to eq 12. The modulation ratio is presented as the frequency-dependent modulation (Maliwal & Lakowicz, 1986):

$$r_\omega = \frac{\Lambda_\omega - 1}{\Lambda_\omega + 2} \quad (18)$$

The anisotropy analysis was performed in two ways. In some cases the total anisotropy (r_0) was held fixed at the value appropriate for no rotational motions. In this case the variable parameters were g_i and θ_i, with $\sum_i g_i = 1.0$. Alternatively, the data were analyzed with the total anisotropy as an unknown, so that the variable parameters were $r_0 g_i = r_i$ and θ_i.

Materials and Methods

Purified preparations of longitudinal sarcoplasmic reticulum ("light") vesicles were obtained from rabbit skeletal muscle as described by Saito et al. (1984). Protein concentration was determined by the method of Lowry et al. (1951), with bovine serum albumin as standard. Calcium binding at equilibrium was measured by a radioactive tracer and chromatography method (Inesi et al., 1980). ATPase activity was determined by following the release of P_i from ATP (Lanzetta et al., 1979), in media containing 0.01 mg of protein/mL, 60 mM MES (pH 6.5), 50 mM KCl, 10 mM $MgCl_2$, 1 mM EGTA, and total calcium to yield the desired concentration of free Ca^{2+} [see Fabiato and Fabiato (1979) for computations], taking care to maintain the desired pH.

Fluorescence intensity was measured with an Aminco-Bowman spectrofluorometer, with 290-nm excitation and 330-nm emission wavelengths. For fluorescence kinetic transients, we used a Dionex D-137 stopped-flow spectrofluorometer, equipped with a 75-W mercury-doped xenon lamp. The excitation wavelength (290 nm) was selected with a monochromator, and the emitted light was passed through a 0-54 Corning cutoff filter. The digitalized signal was collected for storage and analysis. Temperature was controlled at 25 °C. For acrylamide quenching the fluorescence was measured on an SLM 8000 photon counting spectrofluorometer with 298-nm excitation and the emission observed through two broad-band filters, Schott WG 320 and Corning 7-51.

The frequency-domain data were measured on a frequency-domain fluorometer described previously (Lakowicz et al., 1986a,b). The modulated excitation was provided by the harmonic content of a laser pulse train with a repetition rate of 3.79 MHz and a pulse width of 5 ps, from a synchronously pumped and cavity-dumped rhodamine 6G dye laser. The dye

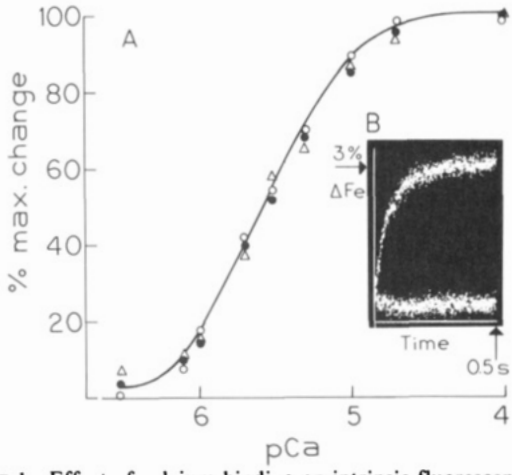

FIGURE 1: Effect of calcium binding on intrinsic fluorescence and activation of sarcoplasmic reticulum ATPase at 25 °C. (A) Ca^{2+} concentration dependence of calcium binding (○), ATPase activity (△), and intrinsic fluorescence rise (●). These measurements were carried out as described under Materials and Methods, following 2–10-min incubation of the SR ATPase with various concentrations of Ca^{2+}. (B) Time dependence of the intrinsic fluorescence rise following addition of saturating Ca^{2+} to ATPase. The experiment was carried out in a stopped-flow fluorometer (see Materials and Methods), mixing a syringe containing 0.3 mg of sarcoplasmic reticulum protein/mL and 1.0 mM EGTA with a syringe containing 1.1 mM $CaCl_2$ and no EGTA. Both syringes contained 60 mM MES (pH 6.5), 50 mM KCl, and 10 mM $MgCl_2$. The maximal change corresponds to 3% of the total fluorescence. The straight horizontal trace was obtained by mixing with no calcium in the second syringe.

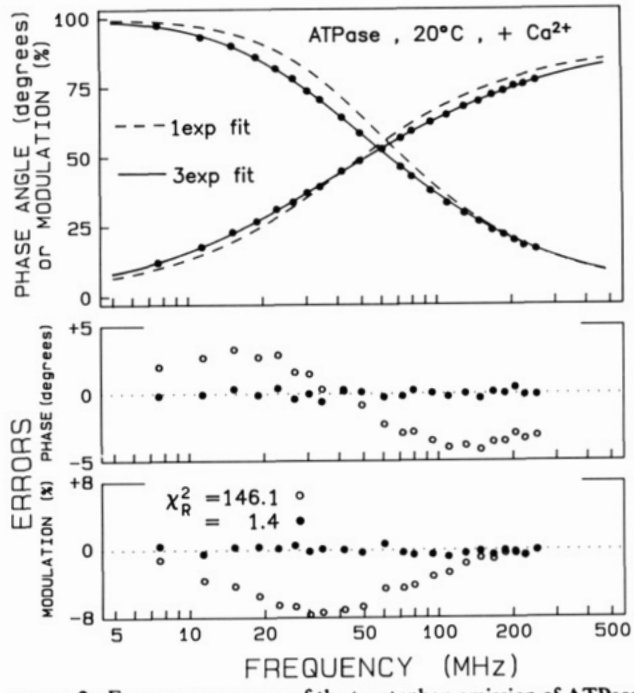

FIGURE 2: Frequency response of the tryptophan emission of ATPase at 20 °C. The dots (●) show the data and the curves the best single- (--) and triple- (—) exponential fits to the data. The lower panels show the deviations between the best single- (○) and triple- (●) exponential fits.

laser was pumped with a mode-locked argon ion laser (Coherent, Innova 15). The dye laser output was frequency doubled to 298 nm with an angle-tuned KDP crystal. The emitted light was observed with a microchannel photomultiplier, and the cross-correlation detection was performed outside the PMT. The emission was observed through a combination of broad-band emission filters, Schott WG 320 and Corning 7-51. For intensity decay measurements, magic-angle polarizer orientations were used.

RESULTS

Concentration and Time Dependence of the Ca^{2+} Effect on Tryptophan Fluorescence. Before proceeding to a full characterization by frequency-domain spectroscopy, we confirmed that our experimental conditions allowed detection of the maximal effect of calcium on the ATPase tryptophan fluorescence, that the observed effect was in fact related to high-affinity calcium binding and enzyme activation, and that our preparation of ATPase displayed the expected increase in tryptophan fluorescence upon binding of Ca^{2+} (Dupont, 1976). Although the ATPase affinity for Ca^{2+} is higher and the binding more cooperative at alkaline pH (Hill & Inesi, 1982), we chose pH 6.5 since the enzyme is more stable and the intrinsic fluorescence signal somewhat stronger at slightly acidic pH. Furthermore, owing to the high binding affinity, we controlled the free Ca^{2+} concentration with an EGTA–Ca buffer. Under these conditions, we measured fluorescence intensity, calcium binding, and ATPase activity as functions of Ca^{2+} concentration. We found that these three parameters have essentially an identical Ca^{2+} concentration dependence within the 10^{-6}–10^{-5} M range, with half-saturation near 3×10^{-6} M Ca^{2+} at pH 6.5 (Figure 1A).

The data shown in Figure 1A were obtained following a several-minute incubation of the enzyme with Ca^{2+}. On the other hand, the time dependence of the tryptophan fluorescence rise following addition of saturating Ca^{2+} to SR ATPase preincubated with EGTA is shown in Figure 1B. It is apparent that the calcium effect is already maximal after 500 ms. On the basis of these measurements, we felt confident that in a few minutes reaction media containing either 2 mM EGTA or 25 μM Ca^{2+} would produce complete depletion or saturation of the specific calcium sites involved in ATPase activation. Therefore, we proceeded to characterize the tryptophan fluorescence under these two sets of experimental conditions.

Tryptophan Intensity Decays of ATPase. We examined the frequency response of the intrinsic tryptophan fluorescence of the ATPase. An example is shown in Figure 2, for ATPase in the presence of Ca^{2+}. As the frequency is increased, one observes increased demodulation, or an increasing phase angle relative to the incident light, that can be used to calculate model-dependent parameters to describe the data (e.g., α_i and Γ_i; see Materials and Methods). The data could not be fit with a single-exponential model, as expected given the presence of multiple tryptophan residues in the ATPase and the known multiexponential decays found even for single tryptophan proteins (Grinvald & Steinberg, 1976; Ross et al., 1981; Beechem & Brand, 1985; Lakowicz et al., 1986a,b). The fits are considerably improved with the double-exponential model, resulting in a decrease in χ_R^2 from about 150 to 3. However, three decay times were required to obtain an adequate fit, resulting in values of χ_R^2 near 1.6 (Table I). With 40 degrees of freedom, a 2-fold decrease in χ_R^2 indicates with 95% confidence that the three decay time model is required (Bevington, 1969). This is consistent with a multiexponential model but does not demonstrate that the decay is uniquely described by three decay times. Hence, we also analyzed the data using a model in which the intensity decay is fit to Lorentzian distributions of decay times (Alcala et al., 1987; James et al., 1987; Lakowicz et al., 1987a). The results of the distribution analysis are shown in Figure 3 and Table II. The data could be fit with a bimodal distribution, resulting in values of χ_R^2 (Table II) which are essentially equivalent to those found with the three decay time model (Table I). This means that the experimental data cannot be used to select either model as

Table I: Multiexponential Analysis of Tryptophan Emission from ATPase

sample	$\bar{\tau}$ (ns)[a]	τ_i (ns)	α_i	f_i	χ_R^2
50 μM Ca^{2+}	4.66	3.76	1.0	1.0	146.1
		2.03	0.548	0.304	
		5.64	0.452	0.696	2.4
		1.40	0.249	0.096	
		3.46	0.564	0.534	
		7.25	0.187	0.370	1.4
no Ca^{2+}	4.59	3.66	1.0	1.0	153.8
		1.90	0.506	0.265	
		5.39	0.494	0.735	2.8
		1.30	0.253	0.091	
		3.52	0.572	0.559	
		7.17	0.175	0.350	1.8
10 mM P_i	4.57	3.63	1.0	1.0	146.4
		1.80	0.471	0.236	
		5.18	0.529	0.764	4.0
		0.95	0.183	0.049	
		3.29	0.645	0.599	
		7.22	0.172	0.352	1.6
50 μM Ca^{2+}/10 mM P_i[b]					4.2
no Ca^{2+}/10 mM P_i					2.1

[a] Calculated from $\bar{\tau} = \sum_i f_i \tau_i$. [b] The data from the first listed sample (before slash) were force fit with the parameters from the three decay time fit for the second listed sample (after slash).

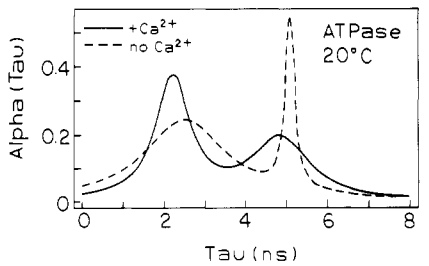

FIGURE 3: Lifetime distributions of the tryptophan emission from ATPase. Distributions are shown with Ca^{2+} (—) and without Ca^{2+} (– –).

correct; both models are consistent with the data. We believe the bimodal distribution model, and in particularly the lifetime distribution plots, provides a useful visualization of the complex intensity decay. It should be noted that the appearance of the lifetime distributions is quite different in the absence and presence of Ca^{2+} (Figure 3).

Also shown in Table II are the χ_R^2 values resulting from the unimodal lifetime distribution fits to the ATPase decays. This simple model with two floating parameters (τ and Γ) provides a surprisingly good fit to the data, which is somewhat superior to the double-exponential model with three variable parameters (τ_1, τ_2, and α_1). This result suggests that there is in fact a distribution of decay times since two discrete decay times are not adequate to represent the data. With our number of degrees of freedom the difference in χ_R^2 between the unimodal and the bimodal fits is adequate to reject the unimodal fit with a certainty of about 80%.

Effect of Ca^{2+} on the ATPase Intensity Decay. A structural effect of Ca^{2+} on the ATPase had been suggested by the small increase in the tryptophan emission observed in the presence of Ca^{2+} (Dupont, 1976; Dupont & Leigh, 1978). It is generally difficult to interpret small changes in fluorescence intensity due to the possibility of changes in the absorption spectrum or concentration of the substance being investigated. In contrast, fluorescence decay times are mostly independent of these experimental factors. Hence, we questioned whether the intensity decay measurements are consistent with the effect of Ca^{2+} on the fluorescence intensity.

The frequency-domain data, in the absence and presence of Ca^{2+}, are shown in Table I. The derived parameters are

Table II: Decay Time Distribution Analysis of Tryptophan Emission from ATPase

sample	τ_i (ns)	Γ_i (ns)	g_i	χ_R^2[a]
50 μM Ca^{2+}	2.21	1.02	0.536	
	4.84	1.73	0.464	1.4 (1.7)
no Ca^{2+}	2.49	2.46	0.813	
	5.07	0.27	0.187	1.8 (2.4)
10 mM P_i	2.40	2.75	0.800	
	4.72	0.52	0.200	2.3 (2.6)
50 μM Ca^{2+}/10 mM P_i[b]				4.3
50 μM Ca^{2+}/no Ca^{2+}				2.6
10 mM P_i/no Ca^{2+}				2.2

[a] The values in parentheses are the values of χ_R^2 found for analysis using a unimodal Lorentzian distribution of decay times. [b] The data from the first sample (before slash) were force fit to the parameters from the fit to the second sample (after slash).

quite similar. Nonetheless, we did observe a small but significant increase in the mean decay time in the presence of Ca^{2+}. In the presence of Ca^{2+} the mean decay time is 4.66 ns, as compared with 4.59 ns without Ca^{2+}; likewise, there is a similar difference between the lifetime-derived intensity parameter ($\sum \alpha_i \tau_i$). It should be noted that the intensity measured directly in the presence of Ca^{2+} increases 3% (Figure 1), which is roughly consistent with the frequency-domain experiments. We emphasize that the increase in mean decay time is experimentally reproducible and statistically significant. The experiment (ATPase ± Ca^{2+}) was repeated several times over the course of 2 years, and addition of Ca^{2+} always resulted in an approximate 2% increase in decay time. Furthermore, we tested whether the data for ATPase + Ca^{2+} were consistent with those for ATPase without Ca^{2+}, and vice versa. This was accomplished by fitting the data for each sample with the three component decay parameters for the alternative sample (Table I). For comparison of the sample with Ca^{2+} with that lacking Ca^{2+}, the value of χ_R^2 increased 3-fold, indicating there is less than a 1% probability that the data represent the same intensity decay. Likewise, the experimental fits to the distribution model (Figure 3 and Table II) show a difference in the presence as opposed to the absence of Ca^{2+}, and attempts to force fit the data from samples with and without Ca^{2+} resulted in an elevated value of χ_R^2. Thus, the results of both the multiexponential and the lifetime distribution models indicate an effect of calcium binding on the intensity decay.

As opposed to the clear effect of Ca^{2+}, we were unable to detect a significant effect of P_i on the fluorescence intensity decay of ATPase tryptophanyl residues. It was previously reported that P_i, under conditions permitting ATPase phosphorylation, produces a very small change of intrinsic fluorescence intensity (Lacapere et al., 1981). Our inability to detect a significant effect in our lifetime studies under appropriate conditions (e.g., pH 6.0, pCa < 8, no K^+) may be related to the very small size of the steady-state intensity change (Lacapere et al., 1981), or to the involvement of only a small fraction of the ATPase tryptophanyl residues.

Acrylamide Quenching of ATPase. We questioned whether the effect of Ca^{2+} on the intensity decay could be the result of an increased lifetime of the single tryptophan (Trp-552) residue known to be present near the nucleotide binding site (MacLennan et al., 1985; Brandl et al., 1986), and therefore within an ATP domain accessible from the cytoplasm. We reasoned that this residue, if present, might be quenched by acrylamide, which is highly soluble in water. Hence, we examined the intensity decays of the ATPase in the presence of increasing amounts of acrylamide, from 0 to 0.5 M (Table III). Representative data are shown in Table III for selected concentrations of acrylamide. The mean decay times are de-

Table III: Effect of Acrylamide on ATPase Intensity Decays

[acrylamide] (M)	$\bar{\tau}$ (ns)	τ_i (ns)	α_i	f_i	χ_R^2
50 μM Ca^{2+}					
0.2	4.15	0.43	0.263	0.041	
		2.70	0.548	0.532	
		6.30	0.187	0.428	1.8
0.4	3.68	0.48	0.341	0.068	
		2.66	0.482	0.528	
		5.57	0.177	0.405	2.5
no Ca^{2+}					
0.2	4.04	0.60	0.282	0.061	
		2.81	0.546	0.550	
		6.33	0.172	0.389	1.4
0.4	3.61	0.48	0.359	0.074	
		2.64	0.489	0.553	
		5.72	0.152	0.373	1.4

creased in the absence and presence of Ca^{2+}. However, the Ca^{2+}-induced difference in the decay times remains evident at all acrylamide concentrations. This suggests that the Ca^{2+} effect is not due to a single residue in a hydrophilic environment or that, if the fluorescence of such a residue is enhanced by Ca^{2+}, this residue is not selectively accessible to acrylamide quenching.

The parameters obtained from the three-exponential fit to the intensity decays in the presence of acrylamide were used to construct Stern–Volmer plots (not shown). The Stern–Volmer quenching constants obtained from either the lifetimes (i.e., $\sum\alpha_i\tau_i$) or the steady-state quantum yields were similar (K_{sv} = 1.6 M^{-1}), indicating that the quenching is dynamic (with no static component). The Stern–Volmer quenching constants are rather small compared to that of a fully exposed residue like *N*-acetyl-L-tryptophanamide (NATA), for which K_{SV} is 17.3 M^{-1} (Eftink & Ghiron, 1977). Hence, the tryptophan residues of ATPase are mostly shielded from contact with the aqueous phase, which is consistent with their dominant presence in the membrane domain of the ATPase. Additionally, the extent of tryptophan exposure to the aqueous phase is not substantially altered by the binding of Ca^{2+}.

The absence of an effect of Ca^{2+} on the acrylamide quenching of the ATPase is consistent with the results of Murphy (1978), who also found no effect of Ca^{2+}. However, our Stern–Volmer constant (1.6 M^{-1}) is 80% less than that reported by Murphy under similar conditions (2.86 M^{-1} from his Figure 3). We are not aware of the origin of this discrepancy and note that our intensity data were corrected for inner-filter effects due to light absorption by acrylamide.

Tryptophan Anisotropy Decays of ATPase. To further elucidate the effect of Ca^{2+} on the ATPase, we examined the tryptophan anisotropy decays (Figure 4). At least two correlation times were required to account for the data (Table IV). The anisotropy decay displays surprising large amplitudes (about 30%) of a subnanosecond component (~0.75 ns). For comparison, we note that this degree of rapid anisotropy loss is comparable to that observed for tetrameric melittin, in which the tryptophan residues are located in a pocket with considerable free volume (Lakowicz et al., 1987a,b; Terwillinger & Eisenberg, 1982). Furthermore, the data could not be fit when the total anisotropy was held constant at the value appropriate for NATA in the absence of rotational diffusion; r_0 = 0.295 at 298-nm excitation. This indicates that there is a component in the anisotropy decay which has not been resolved by our experimental data. One possible origin of this component is motion on the picosecond time scale that could not be recovered with data to 220 MHz. The measurements could not be extended to higher frequencies because the emission is extensively demodulated due to the relatively long

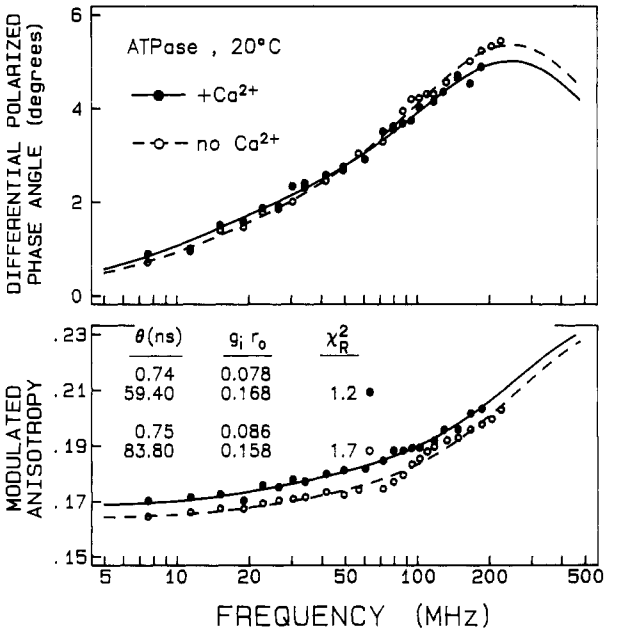

FIGURE 4: Frequency-domain tryptophan anisotropy decays of ATPase.

Table IV: Tryptophan Anisotropy Decays of ATPase

sample	θ_i (ns)	r_0g_i	$\sum r_0g_i$	λ_R^2
50 μM Ca^{2+}	13.12	0.205		137.7
	0.74	0.075		
	59.42	0.168	0.246	1.2
	0.30	0.117		
	38.72	0.178	⟨0.295⟩[a,b]	4.9
	⟨0.75⟩[a]	⟨0.086⟩		
	⟨83.85⟩	⟨0.158⟩	⟨0.244⟩	17.4
no Ca^{2+}	10.90	0.202		208.2
	0.75	0.086		
	83.85	0.158	0.244	1.7
	0.30	0.123		
	39.00	0.172	⟨0.295⟩	9.9

[a] The angular brackets indicate the parameter value was held fixed at the bracketed value. [b] This is the anisotropy of NATA at −60 °C in propylene glycol, 298-nm excitation.

decay times of the tryptophan residues (see Figure 2). Additionally, the emission could not be substantially quenched by acrylamide, so that it was not informative to perform anisotropy measurements on the acrylamide-quenched samples in order to more accurately resolve the short-decay components (Lakowicz et al., 1988a,b). The fact that there are unresolved components is evident from the data (Figure 4). The modulated anisotropy (lower panel) is analogous to the steady-state anisotropy. At low frequencies it is equal to the steady-state anisotropy, and at high frequencies it tends toward the fundamental anisotropy r_0. The data to 200 MHz do not exceed 0.21, indicating incomplete resolution of even the total anisotropy displayed by the samples (0.245). Surprisingly, the data seem to exclude a t = 0 anisotropy value of 0.295, which is expected for isolated and immobile tryptophan residues. This is seen from the 4–6-fold elevation of χ_R^2 when r_0 was held fixed at this value (Table IV).

There are two possible origins for the unresolved portion of the anisotropy decay, picosecond segmental motions and energy transfer among the tryptophan residues. At first glance tryptophanyl energy transfer between the multiple residues seems likely because ATPase contains 13 residues in close proximity, and energy transfer among tryptophan residues is known to occur over distances of about 15 Å (Berlman, 1973; Weber, 1966). However, there are arguments for and against the occurrence of energy transfer in the ATPase. Energy

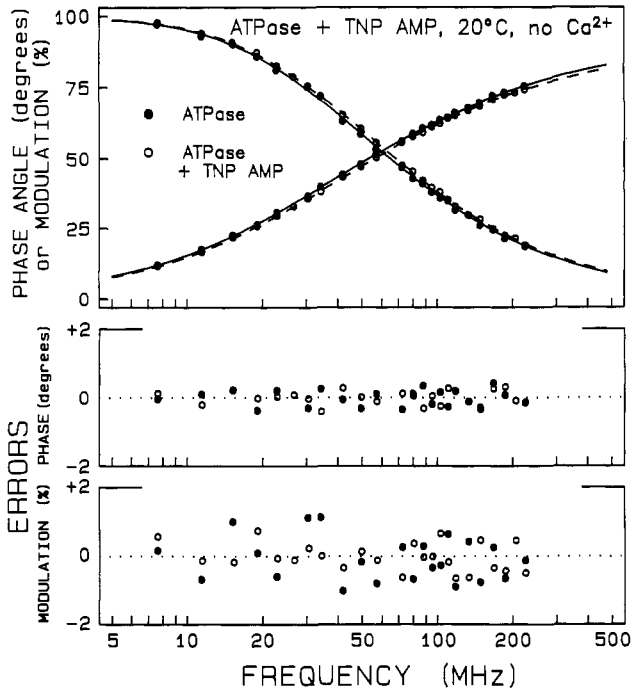

FIGURE 5: Intensity decay of ATPase in the presence of TNP-ATP.

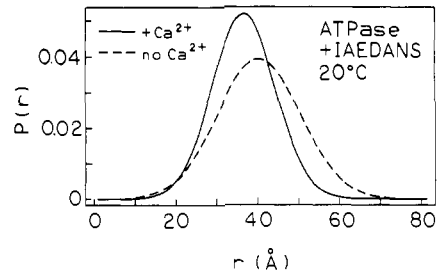

FIGURE 6: Distribution of distances from ATPase tryptophans to IEADANS.

Table V: Multiexponential Analysis in the Presence of TNP-ATP or IEADANS

sample/acceptor	$\bar{\tau}$ (ns)	τ_i (ns)	α_i	f_i	χ_R^2
50 μM Ca^{2+}/TNP-ATP	4.49	1.35	0.267	0.100	
		3.42	0.577	0.565	
		7.22	0.162	0.335	1.0
no Ca^{2+}/TNP-ATP	4.39	0.71	0.157	0.033	
		2.88	0.610	0.519	
		6.44	0.233	0.488	1.0
50 μM Ca^{2+}/IEADANS	3.85	0.53	0.181	0.033	
		2.17	0.418	0.310	
		4.80	0.401	0.657	1.0
no Ca^{2+}/IEADANS	3.78	0.63	0.337	0.078	
		2.61	0.297	0.286	
		4.71	0.366	0.636	1.2

Table VI: Distance Distribution Analysis for ATPase to TNP-ATP or IEADANS

sample/acceptor	R_0 (Å)[a]	$\bar{r}$ (Å)	hw (Å)	χ_R^2
50 μM Ca^{2+}/TNP-ATP	23.6	42.1	13.1	0.9
		39.6	⟨0.1⟩	1.0
		⟨46.5⟩	⟨26.4⟩	1.7
no Ca^{2+}/TNP-ATP	23.2	46.5	26.4	1.3
		38.2	⟨0.1⟩	1.6
50 μM Ca^{2+}/IEADANS	23.0	35.9	17.9	1.0
		32.3	⟨0.1⟩	2.9
		⟨39.6⟩	⟨23.6⟩	5.1
no Ca^{2+}/IEADANS	22.7	39.6	23.6	1.2
		33.7	⟨0.1⟩	2.4

[a] The yields were measured by comparison with tryptophan, 290-nm excitation, a quantum yield of 0.13 being used (Chen, 1967). Forster distances (R_0) were calculated with the standard expression (Lakowicz, 1983; Forster, 1948).

transfer among like fluorophores is known to fail on excitation on the long-wavelength side of the absorption (Weber & Shinitsky, 1970), and our choice of 298-nm excitation results in this condition. However, it is now suspected that the failure of energy transfer requires a shift in the emission spectrum upon long-wavelength excitation and is due to the decrease in spectral overlap which occurs due to this shift. Such shifts only occur in polar solvents of intermediate viscosity (Rubinov & Tomin, 1970; Demchenko, 1986; Lakowicz & Keating-Nakamoto, 1984). Most of the ATPase tryptophan residues are located in a nonpolar environment. Hence, it is possible that energy transfer persists even with 298-nm excitation.

The anisotropy data indicate a significant effect of bound Ca^{2+}. This is initially evident from the increase in modulated anisotropy at low frequency (Figure 4), which is equivalent to an increase in the steady-state anisotropy. The two correlation time analysis indicates that the amplitude of the fast component is decreased from 35% in the absence of Ca^{2+} to 30% with bound Ca^{2+} (Table IV). The difference is significant, as can be seen from our attempt to fit the data for Ca^{2+}-ATPase with the anisotropy decay parameters for the calcium-free ATPase. This attempt results in a 14-fold increase in χ_R^2, from 1.2 to 17.4, which is not statistically acceptable with our degrees of freedom. The increase in anisotropy produced by Ca^{2+} suggests a motional constraint of the tryptophans due to Ca^{2+} binding.

Tryptophan to TNP-ATP Energy Transfer. In a parallel set of experiments we studied energy transfer between tryptophan residues (donors) and TNP-AMP (acceptor), which is a fluorescent nucleotide analogue that binds with high affinity to the catalytic site of SR ATPase (Watanabe & Inesi, 1982; Nakamoto & Inesi, 1984). The effect of calcium on the average Forster distance (R_0) is small (23.2 Å increased to 23.6 Å). We examined the tryptophan decays in the presence of bound ATP in an attempt to determine the distance between the tryptophans and the ATP site and to determine whether this distance is altered by Ca^{2+}. The frequency response of the ATPase, with and without bound TNP-ATP, is shown in Figure 5. Evidently, TNP-AMP has only a minor effect on the tryptophan decay kinetics. Nonetheless, a multiexponential analysis of the data does reveal a small decrease in the mean decay times (Tables I and V), amounting to about a 4% energy transfer efficiency. This indicates that the majority of the tryptophan residues are at a distance of 30 Å or greater from the ATP site. It should also be noted that the extent of energy transfer is not significantly affected by Ca^{2+}. This indicates that Ca^{2+} does not result in a closer spacing between the tryptophan residues and the ATP site, but the data do not exclude the possibility that this distance is increased.

Since the ATPase contains multiple tryptophan residues, we used the data in Table I (donor decays) and Table V (donor–acceptor decays) to calculate the distribution of Trp to TNP-ATP distances. This analysis indicates a wide distribution of distances, in both the presence and absence of Ca^{2+}. The data are also consistent with a narrow distribution as seen from the lack of elevated χ_R^2 values when the hw was held constant at 0.1 Å (Table VI). Similar experiments were performed for energy transfer from tryptophan to IEADANS labels on Cys-670 and -674 (Bishop et al., 1988), which are thought to reside on the cytoplasmic portion of the ATPase (MacLennan et al., 1985). In this case the extent of energy transfer was somewhat larger, around 20% (Table V). These

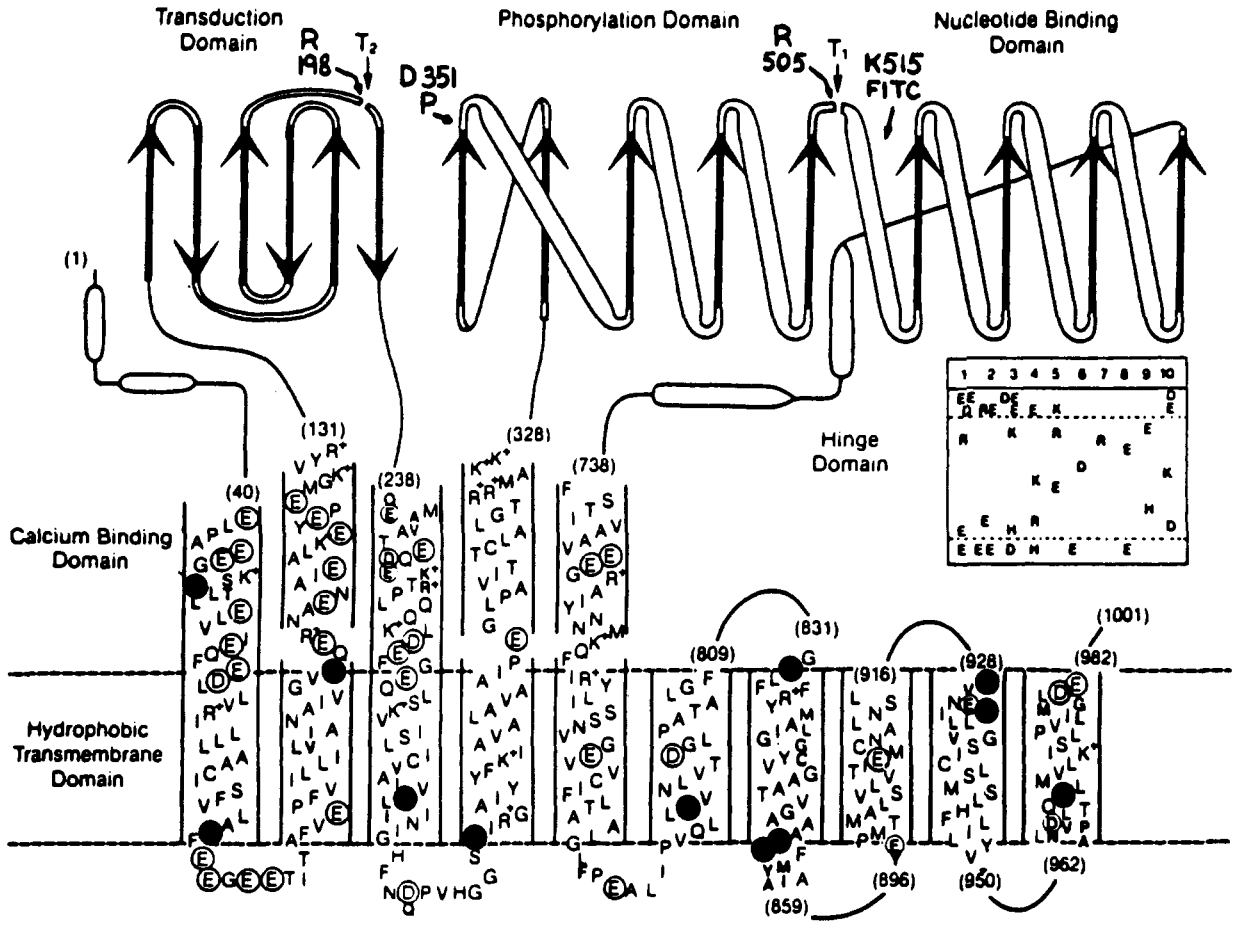

FIGURE 7: Diagram of the ATPase secondary structure derived from sequence analysis (MacLennan et al., 1985; Brandl et al., 1986). Tryptophanyl residues near the membrane interface are shown with filled circles and acid residues with empty circles. Trp-552 (not shown here) is the only tryptophan residue in the cytoplasmic portion of the protein.

data also indicate a sharpening of the distribution in the presence of Ca^{2+} (Figure 7), as was suggested in the results for transfer to TNP-ATP (Table VI). In the case of IEADANS, the data more strongly support the distribution analysis in that the values of χ_R^2 are elevated severalfold when the *hw* is held constant at 0.1 Å (Table VI). The distance distribution analysis yields a sharper peak in the presence of calcium, which is analogous to the calcium effect noted on the distribution of lifetimes. These findings indicate that the majority of tryptophan residues are not in immediate proximity to the nucleotide site. The sharper distance distribution observed in the presence of calcium may be related to the reduction of chain flexibility upon calcium binding.

Discussion

The rise of tryptophan fluorescence intensity produced by calcium binding to the SR ATPase (Dupont, 1976; Dupont & Leigh, 1978) is specifically related to enzyme activation and calcium transport, as demonstrated by the calcium concentration dependence and the kinetic behavior of these phenomena (Guillain et al., 1982; Fernandez-Belda et al., 1984). Likewise, numerous calcium-induced conformational changes have been suggested by various labeling and spectroscopic studies (Murphy, 1978; Ikemoto et al., 1978; Coan & Inesi, 1977). However, their relationship to specific structural features of the Ca-ATPase is unclear, as there is no significant change of ellipticity following the addition of calcium to the SR ATPase (Nakamoto & Inesi, 1986).

We have resolved a calcium-dependent change in the intensity decay of the Ca-ATPase, irrespective of the model assumed to describe the data (i.e., multiexponential or a Lorentzian distribution of decay times). The observed fluorescence decay kinetics (Figure 2), together with the multiexponential and bimodal distribution analysis (Tables I and II and Figure 3), could be attributed to different decay characteristics of various tryptophans. On the other hand, even single tryptophan proteins are known to yield intensity decays that are best fit by a multiexponential decay (Lakowicz et al., 1987a,b), evidently due to the influence of the protein conformation on the decay of the tryptophan (Gryczynski et al., 1988). However, the calcium-dependent increase in the fluorescence yield of the Ca-ATPase is accompanied by a change in the distribution of lifetimes (Figure 3), suggesting the involvement of several, rather than a single, tryptophans. Furthermore, the change in the distribution of Forster distances derived from measurements of energy transfer between tryptophan and either TNP-AMP or IEADANS (Figure 6) implies that calcium binding affects multiple tryptophan residues that are relatively distant from either TNP-AMP, in the nucleotide site, or IEADANS. Since these energy-transfer acceptors are themselves widely separated within the cytoplasmic region of the ATPase (Squier et al., 1987; Bishop et al., 1988), and the tryptophan residues are relatively inaccessible to water-soluble quenchers (Table III and related discussion), it is apparent that the calcium-sensitive tryptophan residues are located in or near the hydrophobic portion of the ATPase. This is in agreement with previous work involving the analysis of the primary sequence in terms of secondary structure (MacLennan et al., 1985; Brandl et al., 1986) in which 12 of the 13 tryptophan residues are predicted to be located on helical segments, near both surfaces of the membrane bilayer (Figure 7). Likewise, the spectroscopic characteristics of

fluorescence emission indicate that most tryptophans reside in a hydrophobic environment (Restall et al., 1986), and it was argued that the calcium-dependent increase in the fluorescence intensity involves these residues, since a much smaller effect is observed in the presence of quenchers that are expected to partition into the hydrophobic phase (Champeil et al., 1986). The calcium effect is not significantly affected by the water-soluble quencher acrylamide (Table III), demonstrating that the single tryptophan residue located near the nucleotide binding domain of the ATPase (i.e., Trp-552) within the large cytoplasmic portion of the membrane is not sensitive to calcium binding.

The calcium-dependent increase in quantum yield is virtually the same (i.e., 2–3%), irrespective of whether the quantum yield is measured by steady-state or lifetime measurements (Figure 1 and Table I). This indicates that the change in fluorescence intensity upon calcium binding is not the result of the modulation of a statically quenched component but most probably involves an alteration in the dynamics of tryptophan residues. This interpretation is supported by the large change in the anisotropy decays (Figure 4 and Table IV) coincident with calcium binding that indicates the tryptophans become more motionally restricted. This effect can be related to the ATPase folding pattern if we consider that nearly all tryptophan residues are thought to be located on the helical segments spanning the membrane, near the surfaces of the membrane bilayer (Figure 7), and in close proximity to a large number of negatively charged residues that are likely to be involved in the formation of divalent cation binding domains (MacLennan et al., 1985; Green et al., 1986). Our present study indicates that calcium binding to the ATPase results in a reduced flexibility of the clustered helices and stabilization of neighboring tryptophans, where the transmembrane helices are likely to be involved in channel formation.

Registry No. ATPase, 9000-83-3; L-Trp, 73-22-3; Ca, 7440-70-2.

References

Alcala, J. R., Gratton, E., & Prendergast, F. G. (1987) *Biophys. J. 51*, 925–936.

Berlman, I. B. (1973) *Energy Transfer Parameters of Aromatic Compounds*, pp 253–254, Academic Press, New York.

Bevington, P. R. (1969) *Data Reduction and Error Analysis for the Physical Sciences*, pp 320–323, McGraw-Hill, New York.

Bishop, J. E., Squier, T. C., Bigelow, D. J., & Inesi, G. (1988) *Biochemistry 27*, 5233–5240.

Brandl, C. J., Green, N. M., Korczack, B., & MacLennan, D. H. (1986) *Cell 44*, 597–607.

Champeil, P., LeMaire, M., Moller, J., Riolett, S., Guillain, F., & Green, N. M. (1986) *FEBS Lett. 206*, 93–98.

Chen, R. F. (1967) *Anal. Lett. 1*, 35–42.

Coan, C., & Inesi, G. (1977) *J. Biol. Chem. 252*, 3044–3049.

Demchenko, A. P. (1986) *Ultraviolet Spectroscopy of Proteins*, Springer-Verlag, Berlin.

Dupont, Y. (1976) *Biochem. Biophys. Res. Commun. 71*, 544–550.

Dupont, Y., & Leigh, J. (1978) *Nature (London) 273*, 396–398.

Eftink, M. R., & Ghiron, C. A. (1977) *Biochemistry 16*, 5546–5551.

Fabiato, A., & Fabiato, F. (1979) *J. Physiol. (Paris) 75*, 463–505.

Fernandez-Belda, F., Kurzmack, M., & Inesi, G. (1984) *J. Biol. Chem. 259*, 9687–9698.

Forster, Th. (1948) *Ann. Phys. 2*, 55–75.

Garcia de Ancos, J., & Inesi, G. (1988) *Biochemistry 27*, 1793–1803.

Gratton, E., & Limkeman, M. (1983) *Biophys. J. 44*, 315–324.

Gratton, E., Lakowicz, J. R., Maliwal, B., Cherek, H., Laczko, G., & Limkeman, M. (1984) *Biophys. J. 46*, 479–486.

Green, N. M., Taylor, W. R., Brandl, C., Korzack, B., & MacLennan, D. (1986) in *Calcium and the Cell*, Ciba Symposium 122, pp 94–113, Wiley, Chicester.

Grinvald, A., & Steinberg, I. Z. (1976) *Biochim. Biophys. Acta 427*, 663–678.

Gryczynski, I., Eftink, M., & Lakowicz, J. R. (1988) *Biochim. Biophys. Acta 954*, 244–252.

Guillain, F., Gingold, M., & Champeil, F. (1982) *J. Biol. Chem. 257*, 7366–7371.

Hill, T., & Inesi, G. (1982) *Proc. Natl. Acad. Sci. U.S.A. 79*, 3978–3982.

Ikemoto, N., Morgan, T., & Yamada, S. (1978) *J. Biol. Chem. 253*, 8027–8033.

Inesi, G. (1985) *Annu. Rev. Physiol. 47*, 573–601.

Inesi, G., Kurzmack, M., Coan, C., & Lewis, D. (1980) *J. Biol. Chem. 255*, 3025–3031.

Klein, U. K. A. (1984) *Arabian J. Sci. Eng. 9*, 327–344.

Lacapere, J., Gingold, M., Champeil, P., & Guillain, F. (1981) *J. Biol. Chem. 256*, 2302–2306.

Lakowicz, J. R. (1983) *Principles of Fluorescence Spectroscopy*, Chapter 10, pp 303–339, Plenum Press, New York.

Lakowicz, J. R., & Maliwal, B. P. (1983) *J. Biol. Chem. 258*, 4794–4801.

Lakowicz, J. R., & Keating-Nakamoto, S. (1984) *Biochemistry 23*, 3013–3021.

Lakowicz, J. R., Maliwal, B., Cherek, H., & Balter, A. (1983) *Biochemistry 22*, 1741–1752.

Lakowicz, J. R., Gratton, E., Laczko, G., Cherek, H., & Limkeman, M. (1984) *Biophys. J. 46*, 463–477.

Lakowicz, J. R., Gryczynski, I., & Cherek, H. (1986a) *J. Biol. Chem. 261*, 2240–2245.

Lakowicz, J. R., Laczko, G., & Gryczynski, I. (1986b) *Rev. Sci. Instrum. 57*, 2499–2506.

Lakowicz, J. R., Cherek, H., Gryczynski, I., Joshi, N., & Johnson, M. L. (1987a) *Biophys. Chem. 28*, 35–50.

Lakowicz, J. R., Johnson, M. L., Wiczk, W., Bhat, A., & Steiner, R. F. (1987b) *Chem. Phys. Lett. 138*, 587–593.

Lakowicz, J. R., Gryczynski, I., Cheung, H. C., Wang, C. K., & Johnson, M. L. (1988a) *Biopolymers 27*, 821–830.

Lakowicz, J. R., Gryczynski, I., & Wiczk, W. M. (1988b) *Chem. Phys. Lett. 149*, 134–139.

Lanzetta, P. A., Alvazez, L. J., Reinsch, P. S., & Candia, D. A. (1979) *Anal. Biochem. 100*, 95–97.

Lowry, D. H., Rosebrough, N. J., Farr, A. L., & Randall, R. J. (1951) *J. Biol. Chem. 193*, 265–275.

MacLennan, D. H., Brandl, C. J., Korczak, B., & Green, N. M. (1985) *Nature (London) 316*, 696–700.

Maliwal, B. P., & Lakowicz, J. R. (1986) *Biochim. Biophys. Acta 873*, 161–172.

Murphy, A. (1978) *J. Biol. Chem. 253*, 385–389.

Nakamoto, R. K., & Inesi, G. (1984) *J. Biol. Chem. 259*, 2961–2970.

Nakamoto, R. K., & Inesi, G. (1986) *FEBS Lett. 194*, 258–262.

Restall, C. J., Coke, M., Philips, E., & Chapman, D. (1986) *Biochim. Biophys. Acta 874*, 305–311.

Ross, J. A. B., Rousslang, K. W., & Brand, L. (1981) *Biochemistry 20*, 4361–4369.

Rubinov, A. N., Tomin, V. I., & Bushuk, B. A. (1982) *J. Lumin. 26*, 377–391.

Saito, A., Seiler, S., Chu, A., & Fleischer, S. (1984) *J. Cell Biol. 99*, 875-885.
Squier, T. C., Bigelow, D. J., Garcia de Ancos, J., & Inesi, G. (1987) *J. Biol. Chem. 262*, 4748-4754.
Steiner, R. F. (1983) *Excited States of Biopolymers*, Chapter 4, pp 117-162, Plenum Press, New York.
Terwillinger, T. C., & Eisenberg, D. (1982) *J. Biol. Chem. 257*, 6016-6022.
Verjovski-Almeida, S. (1981) *J. Biol. Chem. 256*, 2662-2668.
Watanabe, T., & Inesi, G. (1982) *Biochemistry 21*, 3254-3259.
Weber, G. (1966) in *Fluorescence and Phosphorescence Analysis* (Hercules, D. M., Ed.) Chapter 8, pp 217-240, Wiley Interscience, New York.
Weber, G., & Shinitzky, M. (1970) *Proc. Natl. Acad. Sci. U.S.A. 65*, 823-830.

Thermal Unfolding of Myosin Rod and Light Meromyosin: Circular Dichroism and Tryptophan Fluorescence Studies†

Lan King‡ and Sherwin S. Lehrer*

Department of Muscle Research, Boston Biomedical Research Institute, 20 Staniford Street, Boston, Massachusetts 02114, and Department of Neurology, Harvard Medical School, Boston, Massachusetts 02115

Received October 21, 1988; Revised Manuscript Received December 14, 1988

ABSTRACT: Rabbit skeletal myosin rod, which is the coiled-coil α-helical portion of myosin, contains two tryptophan residues located in the light meromyosin (LMM) portion whose fluorescence contributes 27% to the fluorescence of the entire myosin molecule. The temperature dependence of several fluorescence parameters (quantum yield, spectral position, polarization) of the rod and its LMM portion was compared to the thermal unfolding of the helix measured with circular dichroism. Rod unfolds with three major helix unfolding transitions: at 43, 47, and 53 °C, with the 43 and 53 °C transitions mainly located in the LMM region and the 47 °C transition mainly located in the subfragment 2 region. The fluorescence study showed that the 43 °C transition does not involve the tryptophan-containing region and that the 47 °C transition produces an intermediate with different fluorescence properties from both the completely helical and fully unfolded states. That is, although the fluorescence of the 47 °C intermediate is markedly quenched, the tryptophyl residues do not become appreciably exposed to solvent until the 53 °C transition. It is suggested that although the intermediate that is formed in the 47 °C transition contains an extensive region which is devoid of α-helix, the unfolded region is not appreciably solvated or flexible. It appears to have the properties of a collapsed nonhelical state rather than a classical random coil.

Myosin consists of two polypeptide chains each containing a globular head or subfragment 1 (S1) which contains the actin and ATP binding sites, a coiled-coil α-helical rod with a light meromyosin (LMM) region, used in thick filament formation of muscle and a subfragment 2 (S2) region between the head and LMM (Harrington & Rogers, 1984). The LMM and S2 regions of the rod can be isolated after proteolytic digestion (Margossian & Lowey, 1982). Thermal unfolding studies of the rod and its tryptic fragments have indicated that the rod unfolds in several cooperative transitions involving domains along the molecule (Burke et al., 1973; Goodno et al., 1976; Privalov, 1982; Cross et al., 1984; Stafford, 1985) with indications that the most unstable region involves a portion of the subfragment 2 region of the rod near the light meromyosin (LMM)-S2 junction (Burke et al., 1973; Goodno et al., 1976). It is this "hinge" region (Tsong et al., 1979) which was proposed to be involved with the head in reversible force generation (Harrington, 1979).

In this work, we determined that there are two tryptophan residues located in the LMM portion of our preparations of rod purified from rabbit skeletal back muscle and measured the average fluorescence quantum yield. By comparing the temperature dependence of fluorescence properties of rod and LMM with the helix unfolding profiles, we obtained information about the relationship of the domain containing the tryptophans and the intermediates involved in the thermal unfolding. The results indicate that the rod unfolds in three major helix transitions with the least stable region located in the LMM portion not containing the tryptophan residues. The tryptophan fluorescence is sensitive to the unfolding of the two more stable regions, but the fluorescence parameters indicate that the tryptophan environment of the major partly unfolded intermediate is shielded from solvent in contrast to the tryptophan environment of the fully unfolded state, which is fully exposed to solvent.

Experimental Procedures

Rabbit skeletal myosin was prepared by standard procedures as previously outlined (Sreter et al., 1972), rod and S1 were purified from a chymotryptic digest of myosin (Weeds & Pope, 1977), LMM was purified from a tryptic digestion of rod, and rod and LMM were further purified by chromatography on a Protein Pak glass 200sw gel exclusion column in 0.6 M NaCl,

†Supported by grants from the NIH (HL-2246) and the NSF (PCM-8213053). A preliminary report has been presented (King & Lehrer, 1988).
*Address correspondence to this author at the Department of Muscle Research, Boston Biomedical Research Institute.
‡Present address: Chang Gung Medical College, Taiwan, Republic of China.

0006-2960/89/0428-3498$01.50/0